J. Micropalaeontology, 45, 763–775, 2026
https://doi.org/10.5194/jm-45-763-2026
© Author(s) 2026. This work is distributed under
the Creative Commons Attribution 4.0 License.

Journal of Micropalaeontology
Open Access

Reconstructing Ross Sea cryosphere–ocean variability during the Miocene Climatic Optimum using palynology

Suning Hou[1], Joseph G. Prebble[2], Evi Wubben[1], Laura De Santis[3], Robert McKay[4], Denise K. Kulhanek[5,6], and Francesca Sangiorgi[1]

[1]Department of Earth Sciences, Utrecht University, Utrecht, 3584 CB, the Netherlands
[2]GNS Science, Lower Hutt, New Zealand
[3]National Institute of Oceanography and Applied Geophysics (OGS), Trieste, 34010, Italy
[4]Antarctic Research Centre, Victoria University of Wellington, Wellington 6012, New Zealand
[5]Institute of Geosciences, Kiel University, 24118 Kiel, Germany
[6]Department of Earth Sciences, Binghamton University, Binghamton, NY 13902, USA

Correspondence: Suning Hou (s.hou@uu.nl)

Received: 25 June 2026 – Revised: 27 October 2026 – Accepted: 10 November 2026 – Published: 27 November 2026

Abstract. The fate of the Antarctic Ice Sheet (AIS) under climate warming remains highly debated. Geological evidence from the warm Miocene Climatic Optimum (MCO, ∼17–14.7 Ma) is still limited to a few circum-Antarctic records but generally suggests substantial AIS retreat and reduced or absent sea ice. Yet the magnitude and temporal variability of the cryosphere dynamics within the generally warm MCO remain poorly constrained. Here, we present a marine and terrestrial palynological record from sediments recovered at site U1521 on the outer shelf of the central Ross Sea during the International Ocean Discovery Program (IODP) Expedition 374, spanning portions of the interval ∼17.3–14.5 Ma. Dinoflagellate cysts and freshwater-tolerant and brackish-water algae indicate variable surface ocean temperature, productivity and ice melting related to the transition from a marine-terminated ice sheet (16.3–16.2 Ma) to fully open-ocean peak warmth conditions (16.0 Ma). Terrestrial palynomorphs also indicate alternate cooling and warming phases on the hinterland, closely coupled to ice and ocean dynamics. Persistent vegetation implies continued (at least partially) ice-free terrestrial habitats. These results highlight substantial variability in AIS and ocean conditions during the MCO despite an overall warm climate state.

1 Introduction

If unabated, the rate of ongoing greenhouse gas emissions may lead to an atmospheric CO_2 concentration (pCO_2) of up to approximately 600 parts per million by volume (ppmv) and an average of 3 °C warming by the end of the century (Shepherd et al., 2021). Questions remain on the (in)stability of the Antarctic Ice Sheet (AIS) to these changes and consequently the contribution of its melting to sea level rise. Between 1979 and 2022, the AIS lost on average 109 Gt of ice yr^{-1}, contributing a total of 13.3 mm to sea level rise (Shepherd et al., 2021). In particular, the marine-based ice in the Ross Sea is additionally vulnerable to melting due to combined atmospheric and ocean warming (Lowry et al., 2024; Pritchard et al., 2012). In addition, Antarctic sea ice cover has undergone a pronounced decline in recent years (Eayrs et al., 2021; Wilson et al., 2026). This, together with ice sheet melting, will substantially alter the ocean circulation (Li et al., 2023a).

Geological records provide insights into past AIS variability, especially when considering warmer-than-present periods of time. Aspects of the Miocene Climatic Optimum (MCO, ∼17–14.7 Ma) are often presented as analogues of a possible future climate (Steinthorsdottir et al., 2020), given the pCO_2 of up to 1000 ppmv (CenCO2PIP Consortium, 2023) and 3–7 °C warming, as recorded by the decrease in deep-sea oxygen isotopes ($\delta^{18}O_{benthic}$; Westerhold et al., 2020). Furthermore, the amplitude of $\delta^{18}O_{benthic}$ during the MCO (up to 1.2 ‰ VPDB) likely reflects a

highly variable AIS under this sustained warmth (Rohling et al., 2022; Westerhold et al., 2020).

The variability of the Miocene AIS has been mostly inferred from far-field $\delta^{18}O_{benthic}$ (e.g. Holbourn et al., 2013, 2024; Shevenell et al., 2004), which cannot separate ice volume and deep-ocean temperature signals. Far-field clumped isotopes of benthic foraminifera can provide an independent temperature constraint and suggest a relatively large and stable ice sheet on million-year timescales from the mid to late Miocene (Hou et al., 2023b; Leutert et al., 2021; Meckler et al., 2022; Modestou et al., 2020). However, the sensitivity of the AIS to warming seems to vary regionally, with some areas more prone to melting than others (Pritchard et al., 2012). Glycerol dialkyl glycerol tetraethers (GDGTs)-based sea surface temperatures (SSTs) averaged 2–10 °C around Antarctica at MCO peak warmth, with the Ross Sea remaining cooler than the Wilkes Land margin at this time (Duncan et al., 2022; Levy et al., 2016; Sangiorgi et al., 2018). Although there is a difference in latitude between the two areas, this indicates a substantial regional difference in ice sheet stability, likely linked to the extent of the marine-based ice sheet and influence of Circumpolar Deep Waters. Antarctic SSTs are comparable in absolute values to clumped isotope-based deep-sea temperatures (Hou et al., 2023b; Leutert et al., 2021; Meckler et al., 2022; Modestou et al., 2020); however, GDGTs-based SST estimates are highly dependent on the calibration chosen (Dunkley Jones et al., 2020; Kim et al., 2010; Varma et al., 2023) and, more fundamentally, on the archaeal community composition (Ishii et al., 2026). In this context, studies on Antarctica-proximal records of Miocene age may be useful to reconstruct the ice dynamics of the AIS, even though they are frequently fragmentary due to poor core recovery and the existence of several unconformities (Pérez et al., 2021, 2022). So far, several MCO records have been retrieved by scientific drilling offshore the Antarctic continent. Among these, the Antarctic Drilling Project (ANDRILL, inner shelf) and the recent International Ocean Discovery Program (IODP) Expedition 374 in the Ross Sea (Fig. 1) provided preliminary evidence of a variable Ross ice shelf in the background of the generally ice-free Ross Sea during the MCO (Bombard et al., 2024; Duncan et al., 2022; Levy et al., 2016; Marschalek et al., 2021; McKay et al., 2024; Passchier et al., 2011). In addition, modelling outputs continue to produce results considerably cooler than the warm polar conditions as suggested by available proxy data (Burls et al., 2021). Precipitation has been proposed to play a key role in regulating AIS geometry during the MCO (Bradshaw et al., 2021; Hou et al., 2023b), although with few exceptions both data (Feakins et al., 2012) and modelling outputs (Acosta et al., 2024) are scarce.

Palynology, namely marine and aquatic palynomorphs (dinoflagellate cysts hereafter referred to as dinocysts, freshwater-tolerant and brackish-water algae) and terrestrial palynomorphs (pollen and spores) can provide integrated (sea) ice presence and dynamics, temperature and hydrology. Previous studies have indicated temperate waters, partly vegetated continental margin, with melt water discharge and enhanced precipitation during the MCO, despite these circum-Antarctic palynological records having usually low resolution (Feakins et al., 2012; Hannah, 2006; Pound et al., 2012; Sangiorgi et al., 2018; Warny et al., 2009). Previous palynological study on IODP Expedition 374 site U1521 only covered the onset of the MCO (Marschalek et al., 2021). Here, we extend the marine and terrestrial palynomorph record at site U1521 into the MCO and provide a continuous reconstruction of the Ross ice shelf variability between ∼ 16.3 and 16.0 Ma.

2 Materials and methods

2.1 IODP site U1521 lithology and age model

The Ross Sea is positioned between the Victoria Land on the eastern AIS, bordering the Transantarctic Mountains (TAM) and the western AIS (Fig. 1). IODP site U1521 (75° 41.0′ S, 179° 40.3′ W; 562 m water depth) was drilled to 650.1 m below sea floor (m b.s.f.) in the Pennell Basin on the outer continental shelf of the Ross Sea (McKay et al., 2019) (Fig. 1), where ice probably grounded during glacial maxima as indicated by ice sheet models (Colleoni et al., 2018) and observations on LGM and post-LGM sediments (Prothro et al., 2018). Cores 9R to 66R (80–600 m b.s.f.) consist of a lower (∼ 18 Ma) to mid (∼ 15 Ma) Miocene succession with an average recovery of 63 % (Marschalek et al., 2021; McKay et al., 2019).

Cores 66R to 31R (650–286 m b.s.f.) consist mainly of sandy diamictite and interbedded mudstones (McKay et al., 2024). The diamictite generally forms in an ice-proximal setting during ice sheet advances and retreats. Consequently, this interval is interpreted as an ice-proximal glaciomarine setting (Marschalek et al., 2021; McKay et al., 2024). Cores 43R to 31R (380–286 m b.s.f.) are characterised by increasingly cemented silica or chert nodules, which result from the diagenetic alteration of biogenic silica (Marschalek et al., 2021; McKay et al., 2024). Cores 30R to 9R (286–75 m b.s.f.) consist of bioturbated diatom-bearing/rich mudstones, with rare faint laminations and bivalves (McKay et al., 2019). This interval may represent a glacial minimum, as supported by distinctive diatoms and other fossiliferous strata indicating relatively high biogenic productivity (McKay et al., 2024, 2019). Using the lithology, which is indicative of depositional environments ranging from subglacial proximal to open marine settings, a series of glacial proximity sequences was defined (McKay et al., 2024), shown in Figs. 2–4.

The correlation of the site U1521 stratigraphy to seismic profiles shows that the diamictite layers (380–324 m b.s.f.; 285–210 m b.s.f.) correspond to the distal toe of an ice-proximal grounding zone wedge (GZW) that prograded seaward from the western Ross Sea (eastern AIS) (Fig. S1). This geometry suggests that site U1521 drilled a sequence

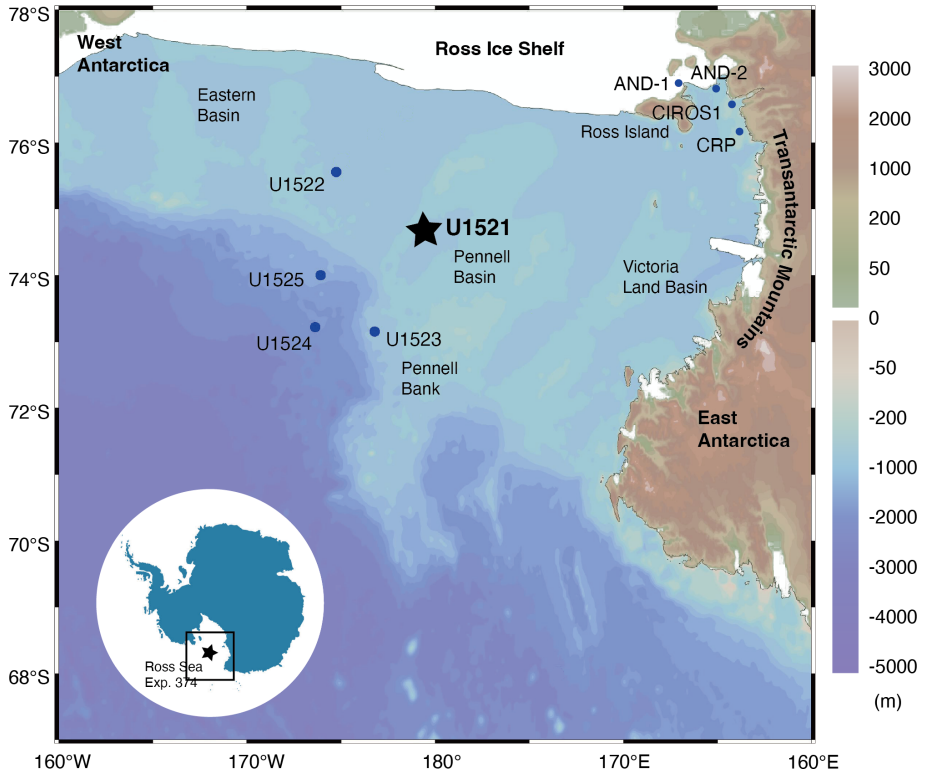

Figure 1. Bathymetric map with locations of IODP 374 site U1521 (star), along with other Expedition 374 sites and ANDRILL cores AND-1 and AND-2 (dot). The figure was created using Ocean Data View (Schlitzer, 2022).

located in the vicinity (seaward) of a morphologic sill, over which ice draining from the eastern AIS-TAM was grounding and fluctuating during the MCO. The mudstone layers (324–285 m b.s.f.; 210–85 m b.s.f.) infill the basin in front of the GZW, which likely has a western AIS origin (Fig. S1 in the Supplement) (Marschalek et al., 2021).

The site U1521 age model used in this study follows McKay et al. (2024) and Marschalek et al. (2021) (Fig. S2). Age constrains consist of magnetostratigraphy, biostratigraphy, cyclostratigraphy, $^{87}Sr/^{86}Sr$ dating of macrofossils, $^{40}Ar/^{39}Ar$ ages of hornblende grains and seismic correlation of regional Ross Sea unconformities (RSUs) (McKay et al., 2024; Pérez et al., 2022). We made a linear regression within each lithological interval using the most reliable magnetostratigraphy datums and the tie lines in McKay et al. (2024) (Fig. S2).

2.2 Palynology

Sample processing was performed in the GeoLab of Utrecht University. Forty-eight sediment samples (∼ 15 g each) were collected from cores 10R to 24R (75–220 m b.s.f.) at a resolution of 1 sample/section (150 cm). Sediments were freeze-dried and then crushed to grains of ∼ 3 mm. *Lycopodium clavatum* ($X = 9666$) tablets were added for the quantification of palynomorph abundances following the method of Wood (1996). Sediment was treated with 10 % hydrochloric acid (HCl) and stored overnight for complete decalcification. After decanting, the samples were centrifuged, and cold 40 % hydrofluoric acid (HF) was added followed by two washes in 30 % HCl for silicate removal. Samples were then sieved through a 250 and a 10 µm sieve, followed by brief immersion in an ultrasonic bath to aid breakup of the organic material. Two microscopic slides were mounted per sample in glycerine jelly with cover slips sealed with nail polish.

In situ and reworked dinocysts, freshwater-tolerant and brackish-water algae (*Cymatiosphaera* spp., *Pediastrum* spp.), and pollen and spores (in situ and reworked) were identified and counted using a microscope with 400× magnification. Dinocyst taxonomy as cited in Williams et al. (2017) and key (Ant)arctic literature (Bijl et al., 2018; Hannah, 2006; Sangiorgi et al., 2009) is followed. Palynological data from an additional 21 samples from cores 25R to 65R (220–600 m b.s.f.) were previously published (Marschalek et al., 2021), using an identical method although the *Lycopodium clavatum* tablets contained a different number of spores ($X = 19\,855$).

Analysis of terrestrial palynomorphs (pollen and spores) on a subset of 53 samples prepared in Utrecht was undertaken at Earth Sciences New Zealand. For terrestrial palynomorphs, 1 slide was examined at 400× magnification, with pollen counts made for an entire slide, or until 100 specimens

were classified. Pollen and spore identification followed taxonomic compilations (Raine et al., 2011; Prebble, 2016), augmented by key Antarctic literature (Askin, 2000; Askin and Raine, 2000; Truswell, 1983).

Dinocysts are grouped into two main groups and identified to genera or species level. Phototrophic gonyaulacoid (G) dinocysts mostly include *Batiacasphaera* spp., *Operculodinium centrocarpum*, *Spiniferites* spp., *Pyxidinopsis* spp. and *Impagidinium pallidum*. Heterotrophic protoperidinioid (P) dinocysts are mostly represented by *Brigantedinium* spp., *Lejeunecysta* spp., *Selenopemphix* spp., *Arcticacysta* spp. and other protoperidinioid cysts, which are generally round, brown and spiny like *Echinidinium* spp. and *Islandinium* spp., and other not yet formally described species (Bijl et al., 2018; McKay et al., 2019; see Plate 1). Among the heterotrophic protoperidinioid dinocysts, *Arcticacysta* spp. and *Selenopemphix antarctica* are usually associated with seasonal sea ice cover (Sangiorgi et al., 2009, 2025; Thöle et al., 2023; Zonneveld et al., 2013). A P/G proxy was calculated by dividing the heterotrophic protoperidinioid dinocyst counts by the sum of protoperidinioid and phototrophic gonyaulacoid dinocyst counts (Fig. S3). Reworked dinocysts concentrations are presented in Marschalek et al. (2021) and not considered further here as they are basically absent in the sediments above 380 m b.s.f.

Percentages of in situ dinocysts and terrestrial palynomorphs were calculated based on the respective totals (Figs. 2, 3). Concentrations (number per gram dry sediment) of dinocyst species, brackish-water algae and terrestrial palynomorphs were calculated by applying the weight of sediment samples and counted *Lycopodium* (Figs. 4, S3).

3 Results

The absolute concentration of in situ marine palynomorphs remains consistently low from 600 to 324 m b.s.f. (Glacial Proximity Sequences 16–10; McKay et al., 2024), at around 300 to 2000 g^{-1} dry sediment (Fig. 4, see also supplementary data) and markedly increases in the upper part of Sequences 9–4. In general, the marine in situ dinocyst assemblages include mainly *Batiacasphaera* spp. (50 %–90 %) and protoperidinioid dinocysts including *Brigantedinium* spp., *Lejeunecysta* spp., and other protoperidinioid species (5 %–65 %) (Fig. 2). Terrestrial palynomorph concentrations remain at around 500 g^{-1} dry sediment, of which *Nothofagidites* spp. is the dominant group, with both *N. lachlaniae* and *N. flemingii* common, and occasional *N. brassii* and *N. asperus* (Figs. 2, 3).

In Sequences 8–5 (285–210 m b.s.f.), the absolute concentration of total palynomorphs is stable at ∼ 5000 g^{-1} dry sediment (Fig. 4), and specimens of the freshwater-tolerant algae *Cymatiosphaera* appears for the first time in the record (Fig. 4). Among the marine dinocysts, *Arcticacysta* spp. reaches 9 %, although phototrophic dinocysts, especially *Batiacasphaera* spp., still dominate the assemblage (Fig. 3). Among the temperate species, *O. centrocarpum* starts to appear, whereas *Spiniferites* spp. are absent. This interval includes the emergence of the distinctive, low-diversity spore and pollen assemblage, including bryophytes (*Coptospora* spp. such as *C. archangelskyi*), *Nothofagidites lachlaniae* and *Tricolpites* sp. A. (Raine, 1998). This assemblage has previously been inferred to originate from a sparse tundra vegetation (e.g. Prebble et al., 2006; Raine, 1998).

The overlying Sequences 5–4 (210–85 m b.s.f.) yield the highest concentration of palynomorphs in the section, reaching 20000 g^{-1} dry sediment (Fig. 4). Both marine and terrestrial palynomorph assemblages appear more variable. There is a notable change observed in the dinocyst assemblage in this interval. In most samples, *Protoperidinium* spp. complex become dominant, whereas *Batiacasphaera* spp. are as low as 10 % (Fig. 3). However, two acmes of *Batiacasphaera* spp. are found at 188 and ∼ 110 m b.s.f. *O. centrocarpum* and *Spiniferites* spp. peak at ∼ 120–100 m b.s.f., reaching ∼ 3000 and 1000 g^{-1} dry sediment, respectively. The base of Sequences 5–4 marks the start of a stepwise increase in the abundance of *Podocarpidites* spp. and *Coptospora* spp., which continues throughout the sequence (Fig. 3). There are marked increases in abundance of *Podocarpidites* spp. at 204, 190 and 132 m b.s.f., when the relative abundance increases from 15 %–30 % to 50 %–60 % of the in situ terrestrial palynomorph assemblage.

4 Discussion

4.1 Sequences 16–10 (600–324 m b.s.f., ∼ 18.6–16.9 Ma)

Sequences 16–10 have been interpreted to have been deposited in an ice-proximal setting by Marschalek et al. (2021). Reworked dinocysts along with West-Antarctica-derived sediments indicate the presence of a marine-based western AIS in this interval (Marschalek et al., 2021; Pérez et al., 2022).

4.2 Sequence 9 (∼ 324–285 m b.s.f.; ∼ 16.9–16.7 Ma)

Sequence 9 is characterised by chert nodules interbedded with silica-cemented mudstone, suggesting an ice-distal depositional environment (Marschalek et al., 2021; McKay et al., 2024, 2019; Pérez et al., 2022). One of our samples from this interval was dominated by protoperidinioid cysts, which we infer reflect nutrient-rich conditions or possibly the presence of sea ice (Harland et al., 1998; Zonneveld et al., 2013) (Figs. 2, 3). Although this interval is relatively sparsely sampled in our study, our results suggest that variable ocean conditions existed within the lithologically homogenous Sequence 9 interval. We interpret the frequent protoperidinioid cysts and the absence of warm-water dinocysts and *Cymatiosphaera* to reflect (ephemeral) relatively cool surface

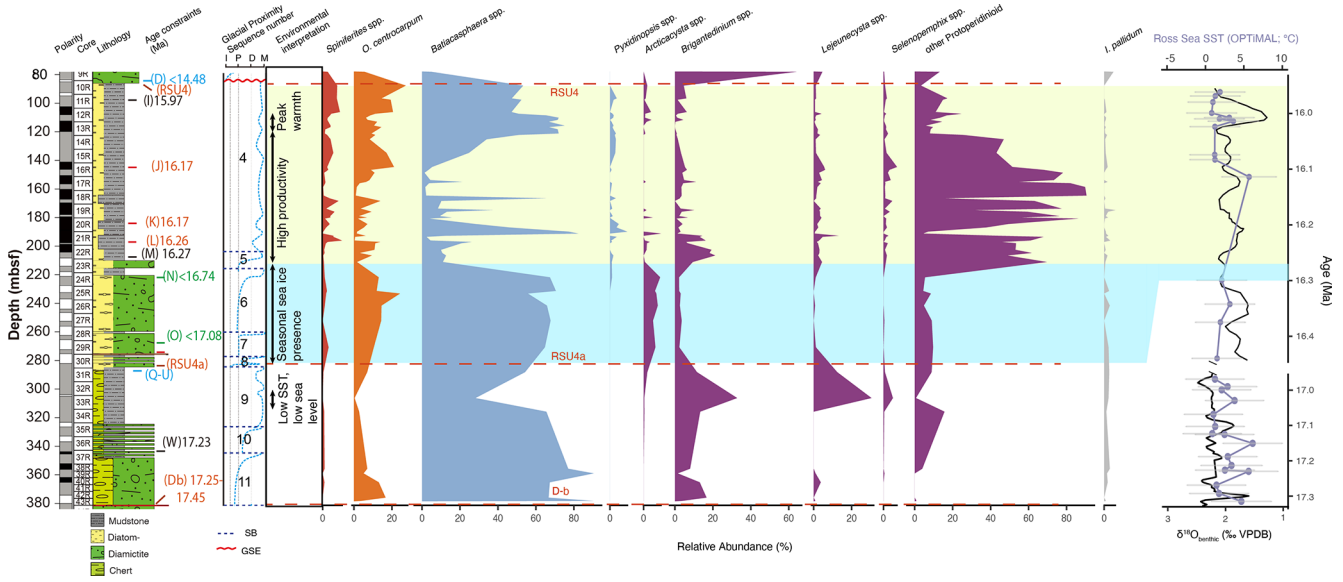

Figure 2. Relative abundance of marine in situ dinoflagellate cysts of the MCO at site U1521. From left to right: depth (metres below sea floor); magnetostratigraphy (black = normal polarity; white = reverse polarity; grey = uncertain polarity or no recovery); core number; lithology; age constraints (McKay et al., 2024); glacial proximity sequences, (blue line; I – ice contact, P – ice proximal, D – ice distal, M – open marine), with non-glacially eroded sequence boundaries (SB; dark-blue dotted line) and glacial surface of erosion sequence boundaries (GSE; wavy red line) (McKay et al., 2024); environmental interpretation based on dinocyst assemblages; dinocyst assemblages orange/reddish = phototrophic warm affinitive dinocyst species; greyish blue = phototrophic dinocyst species likely indicating (seasonally) open ocean conditions; purple = heterotrophic dinocyst species; grey = phototrophic dinocyst typical of polar environment with sea ice (Marret et al., 2020); global $\delta^{18}O_{benthic}$ stack (Westerhold et al., 2020) and Ross Sea sea surface temperature (SST) compilation (Duncan et al., 2022); error bars of SST represent the standard deviation of the temperature estimate (1σ). Dashed red lines denote Ross Sea unconformities (RSUs; Pérez et al., 2021). Yellow and blue polygons indicate age constraints of the highlighted interval.

water and enhanced productivity in the central Ross Sea at 16.79 Ma (304 m b.s.f.). The enhanced productivity was possibly triggered by icebergs calving from the ice sheet and seasonal sea ice formation during this time. It is also the only sample in which *Lejeunecysta* spp. account for over 20 %. This typically coastal genus has previously been reported from the Ross Sea (Hannah et al., 2001; Wrenn et al., 1998), potentially indicating high productivity, shallower waters and more ice-proximal coastal conditions associated with a lower relative sea level. Taken together, the dinocyst assemblage at 304 m b.s.f. suggests a re-advance of the ice sheet.

4.3 Sequences 8–5 (∼ 285–210 m b.s.f.; ∼ 16.3–16.26 Ma)

The marine palynomorph assemblages of Sequences 8–5 are characterised by the onset and regular occurrence of *Arcticacysta* spp. and brackish-water algae *Cymatiosphaera.* spp. *Arcticacysta* spp. reach 9 % of total dinocysts and 150 specimens g^{-1} dry sediment. The extinct *Arcticacysta* spp. was first reported in sediments from the late early Miocene central Arctic Ocean (Sangiorgi et al., 2009); the U1521 record marks the first identification of *Arcticacysta* from the Southern Ocean with a first appearance at ∼ 17.6 Ma and more regular occurrence within the MCO (Sangiorgi et al., 2025). The ecological preference of *Arcticacysta* spp. is still debated as its presence has so far been detected in two records only. In the Arctic record, the presence of *Arcticacysta* spp. is concomitant with freshwater algae and small dropstones (Moran et al., 2006; Sangiorgi et al., 2008). Therefore, sea ice and/or melt water are potentially associated with the occurrence of this taxon. The species belongs to the protoperidinioids; it is therefore likely heterotrophic and may be indicative of high productivity in the Arctic record as *Arcticacysta* spp. are dominant (Sangiorgi et al., 2008, 2009). However, at site U1521, *Arcticacysta* spp. co-exist with dominant phototrophic dinocyst, namely *Batiacasphaera* spp. (Fig. 3). It should be noted that they have a very similar morphology under optical microscopy (Sangiorgi et al., 2009, 2025), and the presence in other records of dinocysts of the genus *Arcticacysta* may have been overlooked. For instance, this genus was found in the North Sea Miocene sediments but not counted separately from *Batiacasphaera* (Kellner et al., 2025).

Sequences 8–5 also continuously contain *O. centrocarpum* (Fig. 4), which suggests that SSTs were relatively high during this phase of the MCO. In modern sediments, *O. centrocarpum* is rarely found south of the Subantarctic Front in the Southern Ocean (e.g. Thöle et al., 2023); therefore, its presence in the Miocene Antarctic ocean suggests a warm/temperate surface ocean (Sangiorgi et al., 2018; Warny et

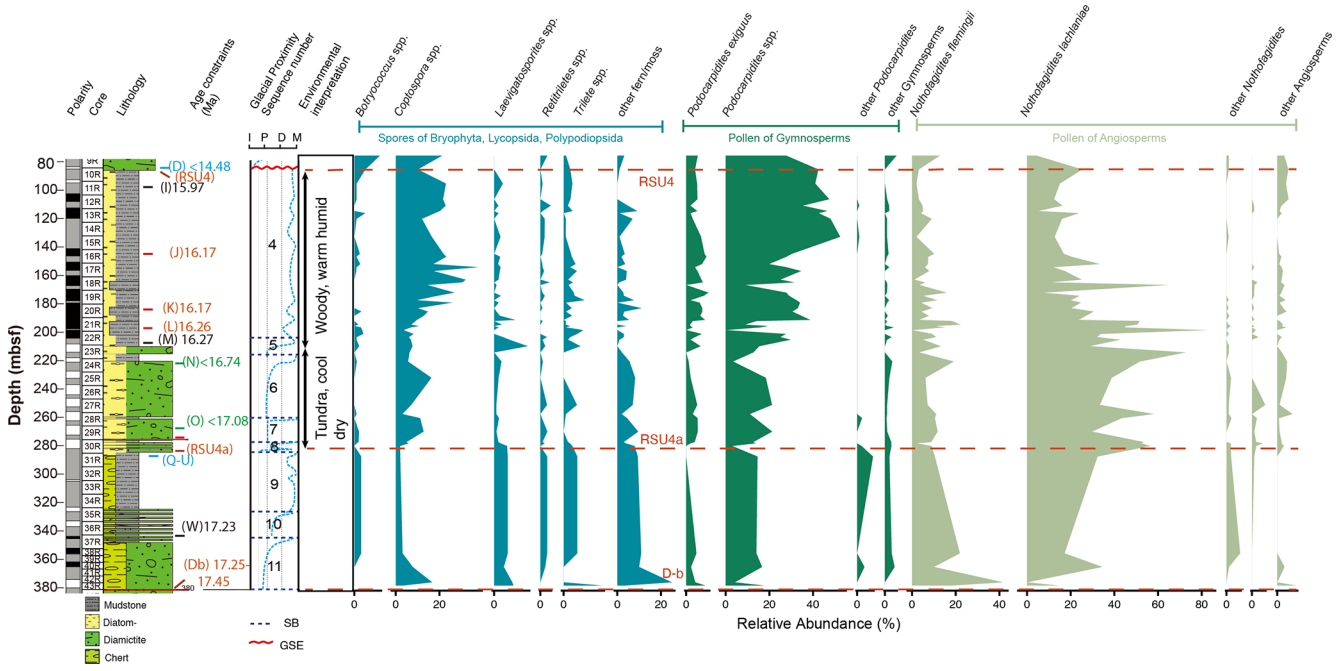

Figure 3. Relative abundance of terrestrial in situ pollen and spores of the MCO at site U1521. From left to right: depth (metres below sea floor); magnetostratigraphy (black = normal polarity; white = reverse polarity; grey = uncertain polarity or no recovery); core number; lithology; age constraints (McKay et al., 2024); glacial proximity sequences (blue line; I – ice contact, P – ice proximal, D – ice distal, M – open marine), with non-glacially eroded sequence boundaries (SB; dotted dark-blue line) and glacial surface of erosion sequence boundaries (GSE; wavy red line) (McKay et al., 2024); environmental interpretation based on pollen and spores; terrestrial palynomorphs are grouped into spores, gymnosperm pollen and angiosperm pollen. Dashed red lines denote Ross Sea unconformities (RSUs; Pérez et al., 2021).

al., 2009). Sequences 8–5 were interpreted as ice grounding line proximal, with marine-based ice sheet advance and retreat cycles (McKay et al., 2024). The proximity of the marine ice front can induce seasonal stratification and consequent surface ocean warming due to (sea) ice melting, as evidenced by the onset of freshwater-tolerant and brackish-water algae (*Cymatiosphaera*) and the dinocyst *Operculodinium* (Fig. 4). In addition, the most notable increase in *Cymatiosphaera* only occurs at the base of the overlying mudstone layer. We therefore interpret the onset of *Cymatiosphaera* in Sequences 8–5 not as evidence for Ross Sea continental ice melting but rather as a result of ice proximity and possibly (sea) ice melting. A tundra vegetation in a dry, temperate-to-cold climate during this time is indicated by abundant *Nothofagidites* spp. and the onset of *Coptospora* spp. (Fig. 3). Compared to Sequence 11 with similar lithology suggesting an ice-proximal setting, the marine-terminating ice sheet in Sequences 8–5 is less stable given the melting and warm/temperate signals from marine palynomorphs.

4.4 Sequences 5–4 (210–85 m b.s.f.; ∼ 16.26–15.8 Ma)

Sequences 5–4 are generally interpreted as open marine deposition and widespread ice retreat (McKay et al., 2024; Pérez et al., 2022). Both marine and terrestrial palynological assemblages are variable in this interval. Here, abundant heterotrophic protoperidinioid dinocysts and abundant diatoms (McKay et al., 2019) in the sediment indicate high productivity surface waters. However, this interval is also characterised by high variability in the dinocyst assemblage, possibly an artifact of the highest sampling resolution. *Batiacasphaera* spp. and protoperidinioid dinocysts alternate in dominance in this interval, which indicates that even within a generally warm phase, productivity and ocean conditions varied remarkably within the ∼ 400 kyr interval (Fig. 3). Productive surface water is suggested by the abundant protoperidinioid cysts but only at times, concurrent with abundant *Cymatiosphaera* spp. (Fig. 4). Protoperidinioid dinocysts such as *Echinidinium* spp. and *Islandinium* spp. are usually considered to be associated with high productivity conditions in surface water (Zonneveld et al., 2013). The concentrations of both protoperidinioid dinocysts and *Cymatiosphaera* blooms in the interval of between 210 and 189 m b.s.f. (∼ 16.26–16.2 Ma), along with elevated *Nothofagidites* spp. on land, suggest sustained melting and freshwater discharge into the Ross Sea. In addition, this interval is the only part that is characterised by coarse sand and gravel clasts in the mudstone interval, which implies the presence of melting-induced ice rafting from a marine-terminating ice sheet in the Ross Sea at that time (McKay et al., 2024). Given the continuous pres-

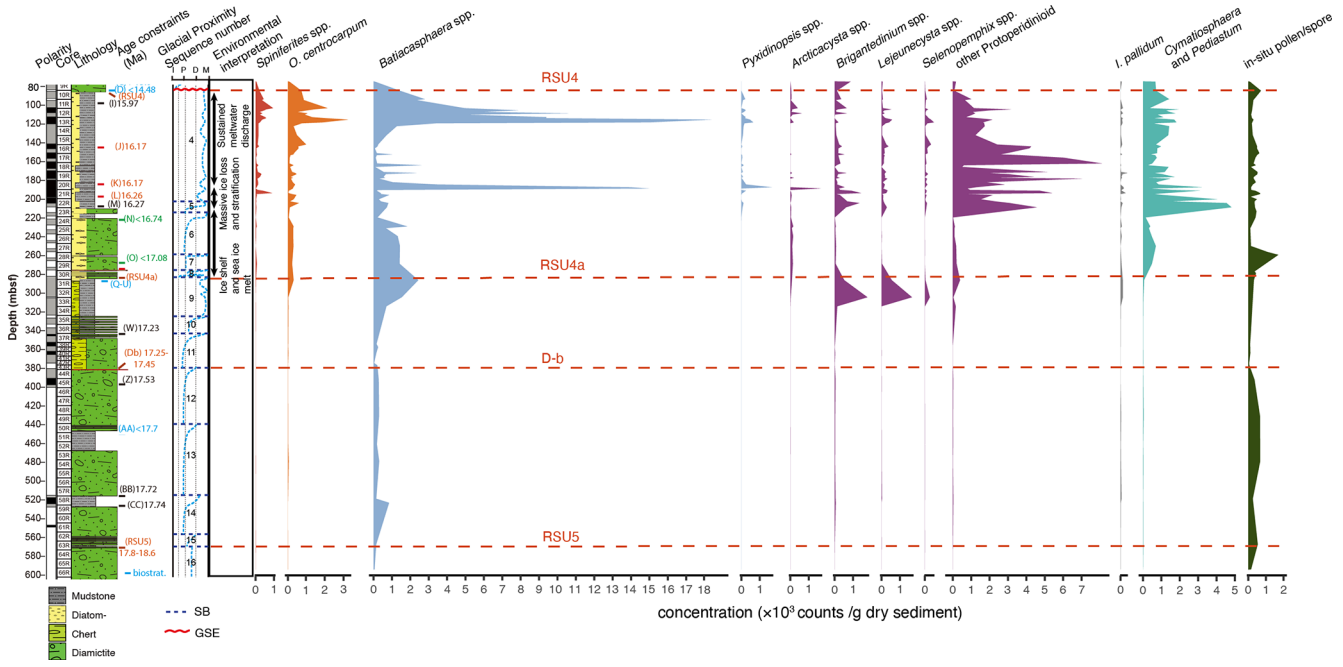

Figure 4. An overview of absolute concentrations of marine dinoflagellate cysts, freshwater-tolerant and brackish-water algae (*Cymatiosphaera* spp. and *Pediastrum* spp.) and terrestrial palynomorphs from core U1521A. From left to right: depth (metres below sea floor); magnetostratigraphy (black = normal polarity; white = reverse polarity; grey = uncertain polarity or no recovery); core number; lithology; age constraints (McKay et al., 2024); glacial proximity sequences (blue line; I – ice contact, P – ice proximal, D – ice distal, M – open marine), with non-glacially eroded sequence boundaries (SB; dotted dark-blue line) and glacial surface of erosion sequence boundaries (GSE; wavy red line) (McKay et al., 2024); environmental interpretation based on brackish-water algae; palynomorph concentrations, dinocyst colour code follows Fig. 2. Cyan = brackish-water algae; dark green = terrestrial palynomorphs. Dashed red lines denote Ross Sea unconformities (RSUs; Pérez et al., 2021).

ence of in situ terrestrial palynomorphs (Figs. 3, 4), even though the ice sheet could be marine terminating, the hinterland around the Ross Sea was likely not completely covered by ice.

The high abundance of heterotrophic protoperidinioid dinocysts is replaced by a peak of over 80 % autotrophic *Batiacasphaera* spp. at ∼ 189 m b.s.f. (16.2 Ma) (Fig. 3). Together with marine *Spiniferites* spp. and *O. centrocarpum*, the assemblage indicates that warm, ice-free open water conditions and low nutrient availability prevailed in the Ross Sea (Thöle et al., 2023; Warny et al., 2009). These observations are also consistent with an inland retreated ice sheet, coincident with the absence of ice-rafted debris (IRD) in the core (McKay et al., 2024). The simultaneous occurrence of abundant *Cymatiosphaera* algae and *Podocarpidites* spp. pollen suggest continuous melt water, stratification and a sustained woody-vegetated humid hinterland (Griener et al., 2015; Thompson et al., 2022) (Fig. 3). The inferred vegetation is consistent with enhanced moisture delivery to the Antarctic coast, as suggested by both leaf wax hydrogen isotopes and modelling (Acosta et al., 2024; Feakins et al., 2012).

Dinocyst assemblages in the interval of 180–130 m b.s.f. (16.18–16.07 Ma) mark another period of high productivity and relatively cooler surface water dominated by heterotrophic dinocysts, comparable to that between 210 and 189 m b.s.f., although it is occasionally interrupted by autotrophic *Batiacasphaera* spp. peaks. However, unlike the 210–189 m b.s.f. interval, this interval is characterised by less abundant *Cymatiosphaera* (Fig. 4) and generally absent IRD (McKay et al., 2024; Zurli et al., 2022). In terms of terrestrial palynomorphs, the spores of mosses (*Coptospora*), which are the first settlers once ice retreats, gradually increase. Collectively, the palynomorphs indicate a retreated of the ice sheet, but the hinterland and surface ocean were relatively cool and the high productivity may have therefore been caused by melt water and/or mixing (Prebble et al., 2006; Sangiorgi et al., 2018; Warny et al., 2009).

A similar *Batiacasphaera*-spp.-dominated interval is found between 120 and 105 m b.s.f. (∼ 16.04–16.00 Ma) (Fig. 2), which corresponds to an MCO warming peak around 16 Ma (Fig. 2). In this interval, warm-affiliated benthic foraminifera taxa *Globocassidulina* and *Gyroidina* were found (Bombard et al., 2024), further emphasising the oceanographic and climatic variability of the MCO.

Oxidation can play a role in the preservation of dinocysts and consequently bias the assemblage, as pigmented protoperidinioid dinocysts are less resistant to oxygenation than gonyaulacoid cysts (Zonneveld et al., 2010). In particular,

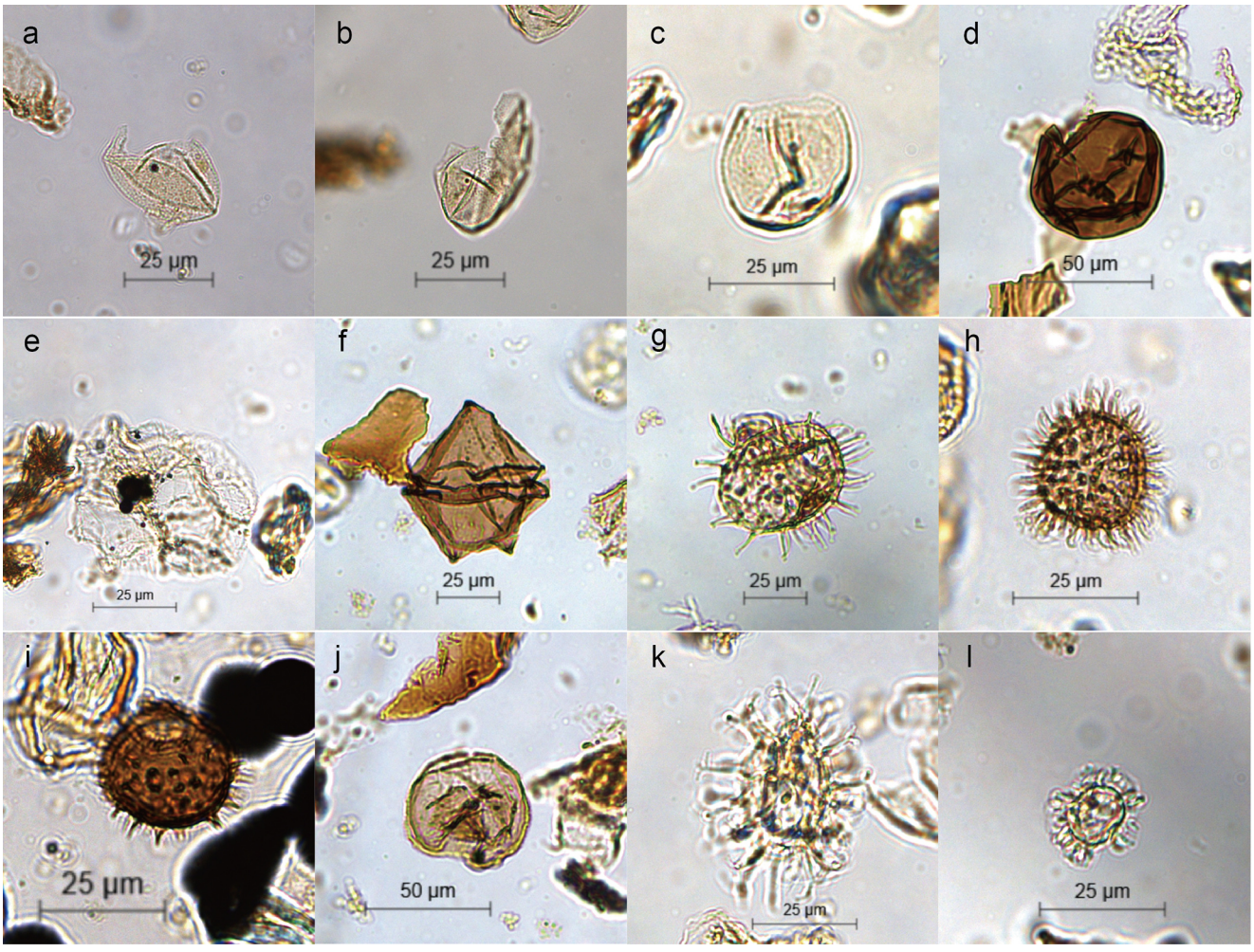

Plate 1. Plate 1 **(a)** *Arcticacysta* sp. 1, U1521A-13R-1W, 10–15 cm; **(b)** *Arcticacysta* sp. 2, U1521A-20R-6W, 18-20 cm; (c) *Batiacasphaera* spp., U1521A-13R-2W, 4–9 cm; **(d)** *Brigantedinium* spp., U1521A-13R-2W, 4–9 cm; **(e)** *Impagidinium pallidum*, U1521A-13R-2W; 4–9 cm; **(f)** *Lejeunecysta acuminata*, U1521A-13R-2W, 4–9 cm; **(g)** *Operculodinium centrocarpum*, U1521A-13R-2W, 4–9 cm; **(h)** *Protoperidinium* sp. 1, U1521A-13R-2W, 4–9 cm; **(i)** *Protoperidinium* sp. 2, U1521A-13R-2W, 4–9 cm; **(j)** *Selenopemphix* spp., U1521A-13R-2W, 4–9 cm; **(k)** *Spiniferites* spp., U1521A-13R-2W, 4–9 cm; **(l)** *Cymatiosphaera* spp., U1521A-22R-3W, 71–76 cm.

during the MCO, increased deep-ocean oxygenation has been reported (Auderset et al., 2022; Hou et al., 2023a) and had a prominent impact on organic carbon preservation (Li et al., 2023b), including both dinocysts and biomarkers, in regions such as in the northern boundary of the Southern Ocean (Hou et al., 2023a, b) and possibly in the Wilkes Land (Sangiorgi et al., 2018). However, the dinocyst assemblage is unlikely to be influenced by oxidation as the total organic carbon of this interval remains relatively high at 1 % (McKay et al., 2019), and the concentration of less-resistant cysts remains relatively high, about 1000 specimens g^{-1} dry sediment. This observation is consistent with the interpretation that globally distributed deep-sea oxidation during the MCO did not occur in the Ross Sea/Pennell Basin, and that deep-water formation may have not been continuously active in this basin at that time (Bombard et al., 2024; Li et al., 2023a; Yamamoto et al., 2015).

Overall, the palynomorphs record phases of ice melting that lead to distinct ocean conditions within the MCO. The earlier phase (210–189 m b.s.f., ∼ 16.26–16.2 Ma) is characterised by a marine-terminating ice sheet retreating to land terminating with iceberg rafting. Iceberg discharge into the ocean resulted in peaks of protoperidinioid dinocysts that indicate local ocean freshening and productivity enhancement. A later phase (∼ 189 and 120–105 m b.s.f., ∼ 16.04–16.00 Ma) is characterised by an ice-free open ocean with only melt water discharge, resulting in dominant gonyaulacoid dinocysts and abundant conifer pollen inferred to originate from a warm open ocean and a humid hinterland, respectively. Throughout this relatively warm interval, we observe periodic changes in the assemblages, which we inter-

pret to reflect periodic small-scale and short-lived cooling, and higher productivity intervals (180–130 m b.s.f.).

5 Conclusion

We reconstruct highly variable surface ocean and terrestrial conditions within the MCO of the West Antarctic margin, Ross Sea, using samples from IODP site U1521. Consistent with lithological evidence, changes in marine dinocysts indicate that the AIS experienced repetitive phases of retreat and advance. However, the deglaciation during the MCO was associated with different surface ocean conditions, alternating between phases of warm/temperate oligotrophic open waters and periods of colder, high nutrient availability. Pollen and spore assemblages indicate the persistent presence of vegetation on the Antarctic hinterland during this time but also show warmer and colder conditions on land. These rapid fluctuations in oceanic, terrestrial and ice conditions provide insights into AIS dynamics under a sustained warm climatic background and call for further studies on millennial-scale AIS variability.

Data availability. All data are available at Zenodo database (https://doi.org/10.5281/zenodo.15852294, Sangiorgi, 2026). Terrestrial palynomorph counting is included in the new version. The seismic data are available at the Antarctic Seismic Data Library System https://scar.org/library-data/data/seismic-data (last access: 26 November 2026).

Supplement. The supplement related to this article is available online at https://doi.org/10.5194/jm-45-763-2026-supplement.

Author contributions. FS designed the research and provided funding. EW conducted the lab work and dinocyst counting. JP conducted the pollen counting. SH revised part of the dinocyst counting, completed the dinocyst record and wrote the paper, with contributions from JP, RM, LDS, DK and FS.

Competing interests. At least one of the (co-)authors is a member of the editorial board of *Journal of Micropalaeontology*. The peer-review process was guided by an independent editor, and the authors also have no other competing interests to declare.

Disclaimer. Publisher's note: Copernicus Publications remains neutral with regard to jurisdictional claims made in the text, published maps, institutional affiliations, or any other geographical representation in this paper. The authors bear the ultimate responsibility for providing appropriate place names. Views expressed in the text are those of the authors and do not necessarily reflect the views of the publisher.

Acknowledgements. This research used data and samples provided by the International Ocean Discovery Program (IODP) and by the Italian National Antarctic Program (PNRA). We thank the IODP Expedition 374 scientists. The seismic line interpretation and correlation with Site U1521 were carried out using the S&P Global Kingdom programme.

Financial support. This research has been supported by the Nederlandse Organisatie voor Wetenschappelijk Onderzoek, Exacte en Natuurwetenschappen to FS (grant no. OCENW.M.21.200), the New Zealand Ministry of Business, Innovation and Employment (grant no. ANTA1801) to JP and RM, the Royal Society of New Zealand Marsden Fund (contract no. MFP-VUW2207) to RM, the PNRA16_00016 project to LDS, and the IODP JOIDES Resolution Science Operator and US National Science Foundation (grant nos. OCE- 1326927 and OPP-2000995) to DK.

Review statement. This paper was edited by Luke Mander and reviewed by Frida Hoem and Damián Cárdenas.

References

Acosta, R. P., Burls, N. J., Pound, M. J., Bradshaw, C. D., De Boer, A. M., Herold, N., Huber, M., Liu, X., Donnadieu, Y., Farnsworth, A., Frigola, A., Lunt, D. J., von der Heydt, A. S., Hutchinson, D. K., Knorr, G., Lohmann, G., Marzocchi, A., Prange, M., Sarr, A. C., Li, X., and Zhang, Z.: A Model-Data Comparison of the Hydrological Response to Miocene Warmth: Leveraging the MioMIP1 Opportunistic Multi-Model Ensemble, Paleoceanogr. Paleoclimatol., 39, e2023PA004726, https://doi.org/10.1029/2023PA004726, 2024.

Askin, R. A.: Spores and Pollen from the Mcmurdo Sound Erratics, Antarctica, in: Paleobiology and Paleoenvironments of Eocene Rocks: McMurdo Sound, East Antarctica, American Geophysical Union (AGU), 161–181, https://agupubs.onlinelibrary.wiley.com/doi/epdf/10.1029/AR076p0161 (last access: 26 November 2026), 2000.

Askin, R. A. and Raine, J. I.: Oligocene and early Miocene terrestrial palynology of the Cape Roberts drillhole CRP-2/2A, Victoria Land Basin, Antarctica, Terra Antartica, 7, 493–501, 2000.

Auderset, A., Moretti, S., Taphorn, B., Ebner, P.-R., Kast, E., Wang, X. T., Schiebel, R., Sigman, D. M., Haug, G. H., and Martínez-García, A.: Enhanced ocean oxygenation during Cenozoic warm periods, Nature, 609, 77–82, https://doi.org/10.1038/s41586-022-05017-0, 2022.

Bijl, P. K., Houben, A. J. P., Hartman, J. D., Pross, J., Salabarnada, A., Escutia, C., and Sangiorgi, F.: Paleoceanography and ice sheet variability offshore Wilkes Land, Antarctica – Part 2: Insights from Oligocene–Miocene dinoflagellate cyst assemblages, Clim. Past, 14, 1015–1033, https://doi.org/10.5194/cp-14-1015-2018, 2018.

Bombard, S. E., Leckie, R. M., Browne, I. M., Shevenell, A. E., McKay, R. M., Harwood, D. M., and the IODP Expedition 374 Scientists: Miocene Climatic Optimum and Middle Miocene Climate Transition: a foraminiferal record from the

central Ross Sea, Antarctica, J. Micropalaeontol., 43, 383–421, https://doi.org/10.5194/jm-43-383-2024, 2024.

Bradshaw, C. D., Langebroek, P. M., Lear, C. H., Lunt, D. J., Coxall, H. K., Sosdian, S. M., and de Boer, A. M.: Hydrological impact of Middle Miocene Antarctic ice-free areas coupled to deep ocean temperatures, Nat. Geosci., 14, 429–436, https://doi.org/10.1038/s41561-021-00745-w, 2021.

Burls, N. J., Bradshaw, C. D., De Boer, A. M., Herold, N., Huber, M., Pound, M., Donnadieu, Y., Farnsworth, A., Frigola, A., Gasson, E., von der Heydt, A. S., Hutchinson, D. K., Knorr, G., Lawrence, K. T., Lear, C. H., Li, X., Lohmann, G., Lunt, D. J., Marzocchi, A., Prange, M., Riihimaki, C. A., Sarr, A. -C., Siler, N., and Zhang, Z.: Simulating Miocene Warmth: Insights From an Opportunistic Multi-Model Ensemble (MioMIP1), Paleoceanogr. Paleoclimatol., 36, https://doi.org/10.1029/2020PA004054, 2021.

CENCO2PIP CONSORTIUM: Toward a Cenozoic history of atmospheric CO2, Science, 382, eadi5177, https://doi.org/10.1126/science.adi5177, 2023.

Colleoni, F., De Santis, L., Montoli, E., Olivo, E., Sorlien, C. C., Bart, P. J., Gasson, E. G. W., Bergamasco, A., Sauli, C., Wardell, N., and Prato, S.: Past continental shelf evolution increased Antarctic ice sheet sensitivity to climatic conditions, Sci. Rep., 8, 11323, https://doi.org/10.1038/s41598-018-29718-7, 2018.

Duncan, B., McKay, R., Levy, R., Naish, T., Prebble, J. G., Sangiorgi, F., Krishnan, S., Hoem, F., Clowes, C., Dunkley Jones, T., Gasson, E., Kraus, C., Kulhanek, D. K., Meyers, S. R., Moossen, H., Warren, C., Willmott, V., Ventura, G. T., and Bendle, J.: Climatic and tectonic drivers of late Oligocene Antarctic ice volume, Nat. Geosci., 15, 819–825, https://doi.org/10.1038/s41561-022-01025-x, 2022.

Dunkley Jones, T., Eley, Y. L., Thomson, W., Greene, S. E., Mandel, I., Edgar, K., and Bendle, J. A.: OPTiMAL: a new machine learning approach for GDGT-based palaeothermometry, Clim. Past, 16, 2599–2617, https://doi.org/10.5194/cp-16-2599-2020, 2020.

Eayrs, C., Li, X., Raphael, M. N., and Holland, D. M.: Rapid decline in Antarctic sea ice in recent years hints at future change, Nat. Geosci., 14, 460–464, https://doi.org/10.1038/s41561-021-00768-3, 2021.

Feakins, S. J., Warny, S., and Lee, J.-E.: Hydrologic cycling over Antarctica during the middle Miocene warming, Nat. Geosci., 5, 557–560, https://doi.org/10.1038/ngeo1498, 2012.

Griener, K. W., Warny, S., Askin, R., and Acton, G.: Early to middle Miocene vegetation history of Antarctica supports eccentricity-paced warming intervals during the Antarctic icehouse phase, Global Planet. Change, 127, 67–78, https://doi.org/10.1016/j.gloplacha.2015.01.006, 2015.

Hannah, M. J.: The palynology of ODP site 1165, Prydz Bay, East Antarctica: A record of Miocene glacial advance and retreat, Palaeogeogr. Palaeoclim., 231, 120–133, https://doi.org/10.1016/j.palaeo.2005.07.029, 2006.

Hannah, M. J., Wrenn, J. H., and Wilson, G. J.: Preliminary Report on Early Oligocene and Latest Eocene Marine Palynomorphs from CRP-3 Drillhole, Victoria Land Basin, Antarctica, Terra Antartica, 8, 383–388, 2001.

Harland, R., Pudsey, C. J., Howe, J. A., and Fitzpatrick, M. E. J.: Recent dinoflagellate cysts in a transect from the Falkland trough to the Weddell Sea, Antarctica, Palaeontology, 41, 1093–1131, 1998.

Holbourn, A., Kuhnt, W., Clemens, S., Prell, W., and Andersen, N.: Middle to late Miocene stepwise climate cooling: Evidence from a high-resolution deep water isotope curve spanning 8 million years: MIOCENE BENTHIC ISOTOPES, Paleoceanography, 28, 688–699, https://doi.org/10.1002/2013PA002538, 2013.

Holbourn, A., Kuhnt, W., Kulhanek, D. K., Mountain, G., Rosenthal, Y., Sagawa, T., Lübbers, J., and Andersen, N.: Re-organization of Pacific overturning circulation across the Miocene Climate Optimum, Nat. Commun., 15, 8135, https://doi.org/10.1038/s41467-024-52516-x, 2024.

Hou, S., Lamprou, F., Hoem, F. S., Hadju, M. R. N., Sangiorgi, F., Peterse, F., and Bijl, P. K.: Lipid-biomarker-based sea surface temperature record offshore Tasmania over the last 23 million years, Clim. Past, 19, 787–802, https://doi.org/10.5194/cp-19-787-2023, 2023a.

Hou, S., Stap, L. B., Paul, R., Nelissen, M., Hoem, F. S., Ziegler, M., Sluijs, A., Sangiorgi, F., and Bijl, P. K.: Reconciling Southern Ocean fronts equatorward migration with minor Antarctic ice volume change during Miocene cooling, Nat. Commun., 14, 7230, https://doi.org/10.1038/s41467-023-43106-4, 2023b.

Ishii, H., Seki, O., Yamamoto, M., and Duncan, B.: New isoprenoid GDGT index as a water mass and temperature proxy in the Southern Ocean, Clim. Past, 22, 585–604, https://doi.org/10.5194/cp-22-585-2026, 2026.

Kellner, L., Dybkjær, K., Piasecki, S., Fredborg, J., Peterse, F., Rasmussen, E. S., Vieira, M., Castro, L., and Śliwińska, K. K.: Early to Middle Miocene in the North Sea Basin: proxy-based insights into environment, depositional settings and sea surface temperature evolution, J. Micropalaeontol., 44, 509–539, https://doi.org/10.5194/jm-44-509-2025, 2025.

Kim, J.-H., van der Meer, J., Schouten, S., Helmke, P., Willmott, V., Sangiorgi, F., Koç, N., Hopmans, E. C., and Damsté, J. S. S.: New indices and calibrations derived from the distribution of crenarchaeal isoprenoid tetraether lipids: Implications for past sea surface temperature reconstructions, Geochim. Cosmochim. Ac., 74, 4639–4654, https://doi.org/10.1016/j.gca.2010.05.027, 2010.

Leutert, T. J., Modestou, S., Bernasconi, S. M., and Meckler, A. N.: Southern Ocean bottom-water cooling and ice sheet expansion during the middle Miocene climate transition, Clim. Past, 17, 2255–2271, https://doi.org/10.5194/cp-17-2255-2021, 2021.

Levy, R., Harwood, D., Florindo, F., Sangiorgi, F., Tripati, R., von Eynatten, H., Gasson, E., Kuhn, G., Tripati, A., DeConto, R., Fielding, C., Field, B., Golledge, N., McKay, R., Naish, T., Olney, M., Pollard, D., Schouten, S., Talarico, F., Warny, S., Willmott, V., Acton, G., Panter, K., Paulsen, T., Taviani, M., SMS Science Team, Acton, G., Askin, R., Atkins, C., Bassett, K., Beu, A., Blackstone, B., Browne, G., Ceregato, A., Cody, R., Cornamusini, G., Corrado, S., DeConto, R., Del Carlo, P., Di Vincenzo, G., Dunbar, G., Falk, C., Field, B., Fielding, C., Florindo, F., Frank, T., Giorgetti, G., Grelle, T., Gui, Z., Handwerger, D., Hannah, M., Harwood, D. M., Hauptvogel, D., Hayden, T., Henrys, S., Hoffmann, S., Iacoviello, F., Ishman, S., Jarrard, R., Johnson, K., Jovane, L., Judge, S., Kominz, M., Konfirst, M., Krissek, L., Kuhn, G., Lacy, L., Levy, R., Maffioli, P., Magens, D., Marcano, M. C., Millan, C., Mohr, B., Montone, P., Mukasa, S., Naish, T., Niessen, F., Ohneiser, C., Olney, M., Panter, K., Passchier, S., Patterson, M., Paulsen, T., Pekar, S., Pierdominici, S., Pollard, D., Raine, I., Reed, J., Reichelt, L., Riesselman, C., Rocchi, S., Sagnotti, L., Sandroni, S., Sangiorgi,

F., Schmitt, D., Speece, M., Storey, B., Strada, E., Talarico, F., Taviani, M., Tuzzi, E., Verosub, K., von Eynatten, H., Warny, S., Wilson, G., Wilson, T., Wonik, T., and Zattin, M.: Antarctic ice sheet sensitivity to atmospheric CO_2 variations in the early to mid-Miocene, P. Natl. Acad. Sci. USA, 113, 3453–3458, https://doi.org/10.1073/pnas.1516030113, 2016.

Li, Q., England, M. H., Hogg, A. M., Rintoul, S. R., and Morrison, A. K.: Abyssal ocean overturning slowdown and warming driven by Antarctic meltwater, Nature, 615, 841–847, https://doi.org/10.1038/s41586-023-05762-w, 2023a.

Li, Z., Zhang, Y. G., Torres, M., and Mills, B. J. W.: Neogene burial of organic carbon in the global ocean, Nature, 613, 90–95, https://doi.org/10.1038/s41586-022-05413-6, 2023b.

Lowry, D. P., Han, H. K., Golledge, N. R., Gomez, N., Johnson, K. M., and McKay, R. M.: Ocean cavity regime shift reversed West Antarctic grounding line retreat in the late Holocene, Nat. Commun., 15, 3176, https://doi.org/10.1038/s41467-024-47369-3, 2024.

Marret, F., Bradley, L., de Vernal, A., Hardy, W., Kim, S.-Y., Mudie, P., Penaud, A., Pospelova, V., Price, A. M., Radi, T., and Rochon, A.: From bi-polar to regional distribution of modern dinoflagellate cysts, an overview of their biogeography, Mar. Micropaleontol., 159, 101753, https://doi.org/10.1016/j.marmicro.2019.101753, 2020.

Marschalek, J. W., Zurli, L., Talarico, F., van de Flierdt, T., Vermeesch, P., Carter, A., Beny, F., Bout-Roumazeilles, V., Sangiorgi, F., Hemming, S. R., Pérez, L. F., Colleoni, F., Prebble, J. G., van Peer, T. E., Perotti, M., Shevenell, A. E., Browne, I., Kulhanek, D. K., Levy, R., Harwood, D., Sullivan, N. B., Meyers, S. R., Griffith, E. M., Hillenbrand, C.-D., Gasson, E., Siegert, M. J., Keisling, B., Licht, K. J., Kuhn, G., Dodd, J. P., Boshuis, C., De Santis, L., and McKay, R. M.: A large West Antarctic Ice Sheet explains early Neogene sea-level amplitude, Nature, 600, 450–455, https://doi.org/10.1038/s41586-021-04148-0, 2021.

McKay, R., Cockrell, J., Shevenell, A. E., Laberg, J. S., Burns, J., Patterson, M., Kim, S., Naish, T., Harwood, D., Levy, R., Marschalek, J., van de Flierdt, T., Ishino, S., Keisling, B., Sousa, I. M. C. de, Cortese, G., Sangiorgi, F., Leckie, R. M., Dodd, J., Duncan, B., Pérez, L. F., Romans, B. W., Kim, S., Bombard, S., Browne, I., van Peer, T., Seki, O., Colleoni, F., Kulhanek, D., De Santis, L., and IODP Expedition 374 Science Team: Miocene ice sheet dynamics and sediment deposition in the central Ross Sea, Antarctica, GSA Bull., https://doi.org/10.1130/B37613.1, 2024.

McKay, R. M., De Santis, L., Kulhanek, D. K., and Expedition 374 Scientists (Eds.): Ross Sea West Antarctic Ice Sheet History, International Ocean Discovery Program, https://doi.org/10.14379/iodp.proc.374.2019, 2019.

Meckler, A. N., Sexton, P. F., Piasecki, A. M., Leutert, T. J., Marquardt, J., Ziegler, M., Agterhuis, T., Lourens, L. J., Rae, J. W. B., Barnet, J., Tripati, A., and Bernasconi, S. M.: Cenozoic evolution of deep ocean temperature from clumped isotope thermometry, Science, 377, 86–90, https://doi.org/10.1126/science.abk0604, 2022.

Modestou, S. E., Leutert, T. J., Fernandez, A., Lear, C. H., and Meckler, A. N.: Warm Middle Miocene Indian Ocean Bottom Water Temperatures: Comparison of Clumped Isotope and Mg/Ca-Based Estimates, Paleoceanogr. Paleoclimatol., 35, e2020PA003927, https://doi.org/10.1029/2020PA003927, 2020.

Moran, K., Backman, J., Brinkhuis, H., Clemens, S. C., Cronin, T., Dickens, G. R., Eynaud, F., Gattacceca, J., Jakobsson, M., Jordan, R. W., Kaminski, M., King, J., Koc, N., Krylov, A., Martinez, N., Matthiessen, J., McInroy, D., Moore, T. C., Onodera, J., O'Regan, M., Pälike, H., Rea, B., Rio, D., Sakamoto, T., Smith, D. C., Stein, R., St John, K., Suto, I., Suzuki, N., Takahashi, K., Watanabe, M., Yamamoto, M., Farrell, J., Frank, M., Kubik, P., Jokat, W., and Kristoffersen, Y.: The Cenozoic palaeoenvironment of the Arctic Ocean, Nature, 441, 601–605, https://doi.org/10.1038/nature04800, 2006.

Passchier, S., Browne, G., Field, B., Fielding, C. R., Krissek, L. A., Panter, K., Pekar, S. F., and and ANDRILL-SMS Science Team: Early and middle Miocene Antarctic glacial history from the sedimentary facies distribution in the AND-2A drill hole, Ross Sea, Antarctica, Geol. Soc. Am. Bull., 123, 2352–2365, https://doi.org/10.1130/B30334.1, 2011.

Pérez, L. F., Santis, L. D., McKay, R. M., Larter, R. D., Ash, J., Bart, P. J., Böhm, G., Brancatelli, G., Browne, I., Colleoni, F., Dodd, J. P., Geletti, R., Harwood, D. M., Kuhn, G., Laberg, J. S., Leckie, R. M., Levy, R. H., Marschalek, J., Mateo, Z., Naish, T. R., Sangiorgi, F., Shevenell, A. E., Sorlien, C. C., van de Flierdt, T., and International Ocean Discovery Program Expedition 374 Scientists: Early and middle Miocene ice sheet dynamics in the Ross Sea: Results from integrated core-log-seismic interpretation, GSA Bull., 134, 348–370, https://doi.org/10.1130/B35814.1, 2021.

Pérez, L. F., McKay, R. M., De Santis, L., Larter, R. D., Levy, R. H., Naish, T. R., Anderson, J. B., Bart, P. J., Busetti, M., Dunbar, G., Sauli, C., Sorlien, C. C., and Speece, M.: Early to middle Miocene ice sheet dynamics in the westernmost Ross Sea (Antarctica): Regional correlations, Global Planet. Change, 216, 103891, https://doi.org/10.1016/j.gloplacha.2022.103891, 2022.

Pound, M. J., Haywood, A. M., Salzmann, U., and Riding, J. B.: Global vegetation dynamics and latitudinal temperature gradients during the Mid to Late Miocene (15.97–5.33 Ma), Earth-Sci. Rev., 112, 1–22, https://doi.org/10.1016/j.earscirev.2012.02.005, 2012.

Prebble, J. G.: Descriptions and occurences of pollen and spores from New Zealand Cenozoic sediments, GNS Science Internal Report 2016/09, 137 pp., 2016.

Prebble, J. G., Raine, J. I., Barrett, P. J., and Hannah, M. J.: Vegetation and climate from two Oligocene glacioeustatic sedimentary cycles (31 and 24 Ma) cored by the Cape Roberts Project, Victoria Land Basin, Antarctica, Palaeogeogr. Palaeocl., 231, 41–57, https://doi.org/10.1016/j.palaeo.2005.07.025, 2006.

Pritchard, H. D., Ligtenberg, S. R. M., Fricker, H. A., Vaughan, D. G., van den Broeke, M. R., and Padman, L.: Antarctic ice-sheet loss driven by basal melting of ice shelves, Nature, 484, 502–505, https://doi.org/10.1038/nature10968, 2012.

Prothro, L. O., Simkins, L. M., Majewski, W., and Anderson, J. B.: Glacial retreat patterns and processes determined from integrated sedimentology and geomorphology records, Mar. Geol., 395, 104–119, https://doi.org/10.1016/j.margeo.2017.09.012, 2018.

Raine, J. I.: Terrestrial Palynomorphs from Cape Roberts Project Drillhole CRP-1, Ross Sea, Antarctica, Terra Antarctica, 5, 539–548, 1998.

Raine, J. I., Mildenhal, D. C., and Kennedy, E. M.: New Zealand fossil spores and pollen: an illustrated catalogue, http://data.gns.

cri.nz/sporepollen/index.htm (last access: 17 September 2024), 2011.

Rohling, E. J., Foster, G. L., Gernon, T. M., Grant, K. M., Heslop, D., Hibbert, F. D., Roberts, A. P., and Yu, J.: Comparison and Synthesis of Sea-Level and Deep-Sea Temperature Variations Over the Past 40 Million Years, Rev. Geophys., 60, e2022RG000775, https://doi.org/10.1029/2022RG000775, 2022.

Sangiorgi, F.: Data for Dating "Zebra": A subaerial to ultra-shallow marine Lomonosov Ridge at the end of the Oligocene? and for Reconstructing Ross Sea ice-ocean variability during the early and middle Miocene Climatic Optimum using palynology (Version 2), Zenodo [data set], https://doi.org/10.1016/j.margeo.2025.107618, 2026.

Sangiorgi, F., Brumsack, H.-J., Willard, D. A., Schouten, S., Stickley, C. E., O'Regan, M., Reichart, G.-J., Sinninghe Damsté, J. S., and Brinkhuis, H.: A 26 million year gap in the central Arctic record at the greenhouse-icehouse transition: Looking for clues, Paleoceanography, 23, https://doi.org/10.1029/2007PA001477, 2008.

Sangiorgi, F., Brinkhuis, H., and Damassa, S. P.: Arcticacysta: A new organic-walled dinoflagellate cyst genus from the early Miocene? of the central Arctic Ocean, Micropaleontology, 55, 249–258, 2009.

Sangiorgi, F., Bijl, P. K., Passchier, S., Salzmann, U., Schouten, S., McKay, R., Cody, R. D., Pross, J., van de Flierdt, T., Bohaty, S. M., Levy, R., Williams, T., Escutia, C., and Brinkhuis, H.: Southern Ocean warming and Wilkes Land ice sheet retreat during the mid-Miocene, Nat. Commun., 9, 317, https://doi.org/10.1038/s41467-017-02609-7, 2018.

Sangiorgi, F., Wubben, E., Hou, S., and Brinkhuis, H.: Dating "*Zebra*": A subaerial to ultra-shallow marine Lomonosov Ridge at the end of the Oligocene?, Mar. Geol., 489, 107618, https://doi.org/10.1016/j.margeo.2025.107618, 2025.

Schlitzer, R.: Ocean Data View, https://odv.awi.de/ (last access: 17 September 2024), 2022.

Shepherd, A., Ivins, E., Rignot, E., Smith, B., van den Broeke, M., Velicogna, I., Whitehouse, P., Briggs, K., Joughin, I., Krinner, G., Nowicki, S., Payne, A., Scambos, T., Schlegel, N., A, G., Agosta, C., Ahlstrøm, A., Babonis, G., Barletta, V., Bjørk, A., Blazquez, A., Bonin, J., Colgan, W., Csatho, B., Cullather, R., Engdahl, M., Felikson, D., Fettweis, X., Forsberg, R., Gallee, H., Gardner, A., Gilbert, L., Gourmelen, N., Groh, A., Gunter, B., Hanna, E., Harig, C., Helm, V., Hogg, A., Horvath, A., Horwath, M., Khan, S., Kjeldsen, K., Konrad, H., Langen, P., Lecavalier, B., Loomis, B., Luthcke, S., McMillan, M., Melini, D., Mernild, S., Mohajerani, Y., Moore, P., Mottram, R., Mouginot, J., Moyano, G., Muir, A., Nagler, T., Nield, G., Nilsson, J., Noël, B., Otosaka, I., Pattle, M., Peltier, W., Pie, N., Rietbroek, R., Rott, H., Sørensen, L. S., Sasgen, I., Save, H., Scheuchl, B., Schrama, E., Schröder, L., Seo, K.-W., Simonsen, S., Slater, T., Spada, G., Sutterley, T., Talpe, M., Tarasov, L., van de Berg, W. J., van der Wal, W., van Wessem, M., Vishwakarma, B. D., Wagner, T., Wiese, D., Wilton, D., Wouters, B., and Wuite, J.: Antarctic and Greenland Ice Sheet mass balance 1992–2020 for IPCC AR6 (1.0), UK Polar Data Centre, Natural Environment Research Council, UK Research & Innovation [data set], https://doi.org/10.5285/77B64C55-7166-4A06-9DEF-2E400398E452, 2021.

Shevenell, A. E., Kennett, J. P., and Lea, D. W.: Middle Miocene Southern Ocean Cooling and Antarctic Cryosphere Expansion, Science, 305, 1766–1770, https://doi.org/10.1126/science.1100061, 2004.

Steinthorsdottir, M., Coxall, H. K., de Boer, A. M., Huber, M., Barbolini, N., Bradshaw, C. D., Burls, N. J., Feakins, S. J., Gasson, E., Henderiks, J., Holbourn, A. E., Kiel, S., Kohn, M. J., Knorr, G., Kürschner, W. M., Lear, C. H., Liebrand, D., Lunt, D. J., Mörs, T., Pearson, P. N., Pound, M. J., Stoll, H., and Strömberg, C. A. E.: The Miocene: The Future of the Past, Paleoceanogr. Paleoclimatol., 36, https://doi.org/10.1029/2020PA004037, 2020.

Thöle, L. M., Nooteboom, P. D., Hou, S., Wang, R., Nie, S., Michel, E., Sauermilch, I., Marret, F., Sangiorgi, F., and Bijl, P. K.: An expanded database of Southern Hemisphere surface sediment dinoflagellate cyst assemblages and their oceanographic affinities, J. Micropalaeontol., 42, 35–56, https://doi.org/10.5194/jm-42-35-2023, 2023.

Thompson, N., Salzmann, U., López-Quirós, A., Bijl, P. K., Hoem, F. S., Etourneau, J., Sicre, M.-A., Roignant, S., Hocking, E., Amoo, M., and Escutia, C.: Vegetation change across the Drake Passage region linked to late Eocene cooling and glacial disturbance after the Eocene–Oligocene transition, Clim. Past, 18, 209–232, https://doi.org/10.5194/cp-18-209-2022, 2022.

Truswell, E. M.: Recycled Cretaceous and Tertiary pollen and spores in antarctic marine sediments: a catalogue, Palaeontogr. Abt. B, 186, 121–174, 1983.

Varma, D., Hopmans, E. C., van Kemenade, Z. R., Kusch, S., Berg, S., Bale, N. J., Sangiorgi, F., Reichart, G.-J., Sinninghe Damsté, J. S., and Schouten, S.: Evaluating isoprenoidal hydroxylated GDGT-based temperature proxies in surface sediments from the global ocean, Geochim. Cosmochim. Ac., https://doi.org/10.1016/j.gca.2023.12.019, 2023.

Warny, S., Askin, R. A., Hannah, M. J., Mohr, B. A. R., Raine, J. I., Harwood, D. M., Florindo, F., and the SMS Science Team: Palynomorphs from a sediment core reveal a sudden remarkably warm Antarctica during the middle Miocene, Geology, 37, 955–958, https://doi.org/10.1130/G30139A.1, 2009.

Westerhold, T., Marwan, N., Drury, A. J., Liebrand, D., Agnini, C., Anagnostou, E., Barnet, J. S. K., Bohaty, S. M., De Vleeschouwer, D., Florindo, F., Frederichs, T., Hodell, D. A., Holbourn, A. E., Kroon, D., Lauretano, V., Littler, K., Lourens, L. J., Lyle, M., Pälike, H., Röhl, U., Tian, J., Wilkens, R. H., Wilson, P. A., and Zachos, J. C.: An astronomically dated record of Earth's climate and its predictability over the last 66 million years, Science, 369, 1383–1387, https://doi.org/10.1126/science.aba6853, 2020.

Williams, G. L., Fensome, R. A., and MacRae, R. A.: The Lentin and Williams index of fossil dinoflagellates, 2017.

Wilson, E. A., Arlen, L., and Campbell, E. C.: Recent extremes in Antarctic sea ice extent modulated by ocean heat ventilation, P. Natl. Acad. Sci., 123, e2530832123, https://doi.org/10.1073/pnas.2530832123, 2026.

Wood, G. D.: Palynological techniques-processing and microscopy, in: Palynology: Principles and Application, American Association of Stratigraphic Palynologists Foundation, ISBN 9780931871030, 1996.

Wrenn, J. H., Hannah, M. J., and Raine, J. I.: Diversity and Palaeoenvironmental Significance of Late Cainozoic Marine Pa-

lynomorphs from the CRP-l Core, Ross Sea, Antarctica, Terra Antartica, 5, 553–570, 1998.

Yamamoto, A., Abe-Ouchi, A., Shigemitsu, M., Oka, A., Takahashi, K., Ohgaito, R., and Yamanaka, Y.: Global deep ocean oxygenation by enhanced ventilation in the Southern Ocean under long-term global warming, Global Biogeochem. Cy., 29, 1801–1815, https://doi.org/10.1002/2015GB005181, 2015.

Zonneveld, K. A. F., Versteegh, G. J. M., Kasten, S., Eglinton, T. I., Emeis, K.-C., Huguet, C., Koch, B. P., de Lange, G. J., de Leeuw, J. W., Middelburg, J. J., Mollenhauer, G., Prahl, F. G., Rethemeyer, J., and Wakeham, S. G.: Selective preservation of organic matter in marine environments; processes and impact on the sedimentary record, Biogeosciences, 7, 483–511, https://doi.org/10.5194/bg-7-483-2010, 2010.

Zonneveld, K. A. F., Marret, F., Versteegh, G. J. M., Bogus, K., Bonnet, S., Bouimetarhan, I., Crouch, E., de Vernal, A., Elshanawany, R., Edwards, L., Esper, O., Forke, S., Grøsfjeld, K., Henry, M., Holzwarth, U., Kielt, J.-F., Kim, S.-Y., Ladouceur, S., Ledu, D., Chen, L., Limoges, A., Londeix, L., Lu, S.-H., Mahmoud, M. S., Marino, G., Matsouka, K., Matthiessen, J., Mildenhal, D. C., Mudie, P., Neil, H. L., Pospelova, V., Qi, Y., Radi, T., Richerol, T., Rochon, A., Sangiorgi, F., Solignac, S., Turon, J.-L., Verleye, T., Wang, Y., Wang, Z., and Young, M.: Atlas of modern dinoflagellate cyst distribution based on 2405 data points, Rev. Palaeobot. Palyno., 191, 1–197, https://doi.org/10.1016/j.revpalbo.2012.08.003, 2013.

Zurli, L., Perotti, M., and Talarico, F.: Data report: petrology of gravel-sized clasts from Site U1521 core, IODP Expedition 374, Ross Sea West Antarctic Ice Sheet History, https://doi.org/10.14379/iodp.proc.374.201.2022, 2022.